RSC Advances

PAPER

View Article Online
View Journal | View Issue

Cite this: *RSC Adv.*, 2022, **12**, 34404

Luminescence and energy transfer of single-phase white-emitting phosphor $Ba_2Mg(PO_4)_2$:Ce^{3+}, Eu^{2+} for white LEDs†

Tao Wang,*[a] Mingjie Zheng,[b] Zhijun Wang [b] and Panlai Li *[b]

A series of $Ba_2Mg(PO_4)_2$:Ce^{3+}, Eu^{2+} phosphors were synthesized by the traditional high temperature solid-state method, and the crystal structures and luminescence properties of the samples were discussed systematically. The energy transfer from Ce^{3+} to Eu^{2+} in $Ba_2Mg(PO_4)_2$ was proved to be of resonant type *via* a dipole–dipole interaction mechanism. With a precisely controlled relative proportion of Ce^{3+}/Eu^{2+}, the emission color of the samples can vary from blue (0.157, 0.071) to white (0.352, 0.332) and ultimately to yellow (0.452, 0.466) under the 323 nm ultraviolet light radiation excitation. The result reveals that the $Ba_2Mg(PO_4)_2$:Ce^{3+}, Eu^{2+} phosphor may have potential application as a single-phased white-emitting phosphor for light emitting diodes.

Received 9th October 2022
Accepted 25th November 2022

DOI: 10.1039/d2ra06357c

rsc.li/rsc-advances

1. Introduction

In recent years, white light emitting diodes (LEDs) have attracted the attention of domestic and foreign researchers due to their energy saving, high efficiency, long life, and other advantages.[1] At present, white LEDs can be achieved by combining a blue InGaN LED chip with a yellow phosphor, YAG:Ce, which shows a poor color rendering index ($R_a \approx 70$–80) and high CCT (CCT $\approx$ 7750 K) due to a lack of red component.[1] To solve these problems, white LEDs can also be fabricated by near-ultraviolet (UV) LED or UV-LED pumping red/green/blue multi-phased phosphors or a single-phase white emitting phosphor.[2–4] Generally, a white emitting phosphor can be obtained by controlling the concentration of several rare earths, however, due to the lack of certain light components, the obtained white phosphor shows a low color rendering index and cannot be applied in practice.[6–11] Therefore, the discovery of new phosphors, the design of crystal structure and the optimization of luminescence performance are still the hot spots of current research. Actually, the method of obtaining white light phosphor by using two kinds of rare earth ions doped together to generate energy transfer is the most popular among researchers. The phosphor obtained by this method presents a wide spectrum coverage. In addition, since there are only two types of activated ions, there are fewer energy transfer processes and relatively less energy loss. Therefore, this is an ideal method at present. In the process of obtaining single-phase white emitting phosphor, the choice of two kinds of activated particles is also crucial. Generally, the selected activated ions are two rare earth ions or rare earth/transition metal ions. Under the condition of energy level matching, energy transfer can occur between the doped activation ions, such as Ce^{3+}/Eu^{2+}, Ce^{3+}/Mn^{2+} and Eu^{2+}/Mn^{2+}.[2–6] Considering that the luminescence properties of Ce^{3+} and Eu^{2+} ions are relatively good, and the spectral coverage is wide, especially for Eu^{2+} ions, their spectral coverage can be from ultraviolet to near infrared, hence the researchers are more inclined to use Ce^{3+}/Eu^{2+} co-doping to obtain white emission, this work also uses this method to obtain white emitting phosphor.[7–26]

To the best our knowledge, in addition to the selection of activated ions, the matrix materials is also very important. For the host materials of phosphors, phosphate compounds are widely used currently owing to the facile synthesis, environmental-friendly characteristics and high stabilities, such as (Ca, Sr)$_9$Sc(PO$_4$)$_7$:Eu^{2+}, Mn^{2+},[27] $Ca_{9-x-y}Ce(PO_4)_7$:xEu^{2+}, yMn^{2+}[28] and $Ca_9La(PO_4)_7$:Eu^{2+}.[29] $BaMg_2(PO_4)_2$ is an alkaline earth phosphate compound with a rigid tetrahedral three-dimensional structure. Its physical and chemical properties are stable. Although the luminescence performance of $Ba_2Mg(PO_4)_2$:Eu^{2+} has been widely investigated,[30–36] however, a systematic study on the energy transfer between Eu^{2+} and Ce^{3+} in $Ba_2Mg(PO_4)_2$ was not reported. In this work, the crystal structure of $Ba_2Mg(PO_4)_2$ and preferred crystallographic sites for activators were reported. The structure of $Ba_2Mg(PO_4)_2$ is monoclinic with space group $P2_1/n$ ($Z = 4$). There are two Ba^{2+} sites in this crystal lattice, one is 7 coordination, the other is 8 coordination, which can be replaced by rare earth dopants. The luminescence properties of Eu^{2+} and Ce^{3+} in $Ba_2Mg(PO_4)_2$ is

[a]College of Science, China University of Petroleum (East China), Qingdao 266580, China. E-mail: twang@upc.edu.cn

[b]College of Physics Science & Technology, Hebei Key Lab of Optic-Electronic Information and Materials, Hebei University, Baoding 071002, China. E-mail: li_panlai@126.com

† Electronic supplementary information (ESI) available. See DOI: https://doi.org/10.1039/d2ra06357c

demonstrated. After co-doping with Ce^{3+} ions, the emission intensity of Eu^{2+} ions was enhanced and a novel blue-yellow tunable phosphor $Ba_2Mg(PO_4)_2$:Ce^{3+}, Eu^{2+} can be obtained by varying the relative ratio of Ce^{3+}/Eu^{2+} under the irradiation of 323 nm light. Moreover, the energy transfer process and mechanism between Ce^{3+} and Eu^{2+} has been discussed systematically.

2. Experimental section

2.1 Synthesis

A series of $Ba_2Mg(PO_4)_2$:$x$$Ce^{3+}$, $y$$Eu^{2+}$ phosphors were prepared by a traditional high-temperature solid-state method. The raw materials are $BaCO_3$ (99.99%), MgO (99.99%), $NH_4H_2PO_4$ (99.99%), CeO_2 (99.99%) and Eu_2O_3 (99.99%), which thoroughly mix and grind in an agate mortar for 20 min. Then powder mixtures were pre-heated in furnace at 500 °C for 2 h, and subsequently sintered at 1100 °C for 5 h in CO reducing atmosphere to get the final samples. Finally, the furnace temperature was lowered to room temperature, and the phosphor was ground before subsequent characterization.

2.2 Material characterization

The structure of samples is identified by powder X-ray diffraction (Bruker D8 X-ray diffractometer), with Ni-filtered Cu Kα radiation ($\lambda = 0.15405$ nm), operating at 40 mA and 40 kV and recorded the patterns in the range of 2θ from 10° to 80°. The structural refinements were analyzed by General Structural Analysis System (GSAS) program. The steady time photoluminescence spectra including excitation (PLE) and emission (PL) spectra are measured in the range of 240 nm to 800 nm with scanning speed 1200 nm min^{-1} by a HITACHI F-4600 fluorescence spectrometer. The temperature dependent luminescence properties were measured on the same spectrophotometer, which was assembled with a TAP-02 high temperature fluorescence controller. The decay curves of the photoluminescence are acquired by FLS920 fluorescence spectrometer.

3. Results and discussion

3.1 Phase formation and structure of $Ba_2Mg(PO_4)_2$

It was reported that $Ba_2Mg(PO_4)_2$ (BMPO) is member of apatite-type family, which has a monoclinic structure with space group P_12_1/n_1.[37] The crystal structure of BMPO is shown in Fig. 1a. There are two types of Ba ions polyhedrons in this host, and Ba ions polyhedrons are accommodated in the tunnels that come out of three-dimensional framework of MgO_6 and PO_4 tetrahedrons. The Ba_1 is surrounded by eight O atoms and Ba_2 coordinate with seven O atoms. The Rietveld refinement with the results of BMPO presented in Fig. 2b, and the Rietveld refinement method has been conducted with GSAS. More XRD patterns and refined parameters are in Fig. S1 and Table S1,† and the diffraction peaks of the samples are well matched with the standard card BMPO (ICSD#59253), and no other impurity peaks are found, indicating the samples are all single crystal pure phase samples.

3.2 Luminescence properties of $Ba_2Mg(PO_4)_2$:Ce^{3+}

Fig. 2a and b show the emission spectra and excitation spectra of BMPO:$x$$Ce^{3+}$($x$ = 0.003–0.07). It can be seen that under the excitation of 323 nm, the emission spectra of BMPO:$x$$Ce^{3+}$ show an asymmetric emission band with a peak around 407 nm, which originates from the transition from 5d to 4f ground state. The excitation spectrum recorded by monitoring the emission of 407 nm consists of a stronger excitation band centered at 323 nm, and the spectrum goes from 220 nm to 380 nm. The insets of Fig. 2a and b present the emission intensity of Ce^{3+} ions with its concentration, respectively. The intensities both increase with the increase of Ce^{3+} ion content. The intensity reaches the strongest at $x = 0.05$, and then the intensity gradually decreases due to the quenching effect of the activated ions. It is well known that Ce^{3+} emission should be composed of a double band due to the splitting of its 4f ground state, and the energy difference of this splitting between $^2F_{7/2}$ and $^2F_{5/2}$ of Ce^{3+} is about 2000 cm^{-1}. In this study, the asymmetric emission band can be decomposed into two well-separated Gaussian

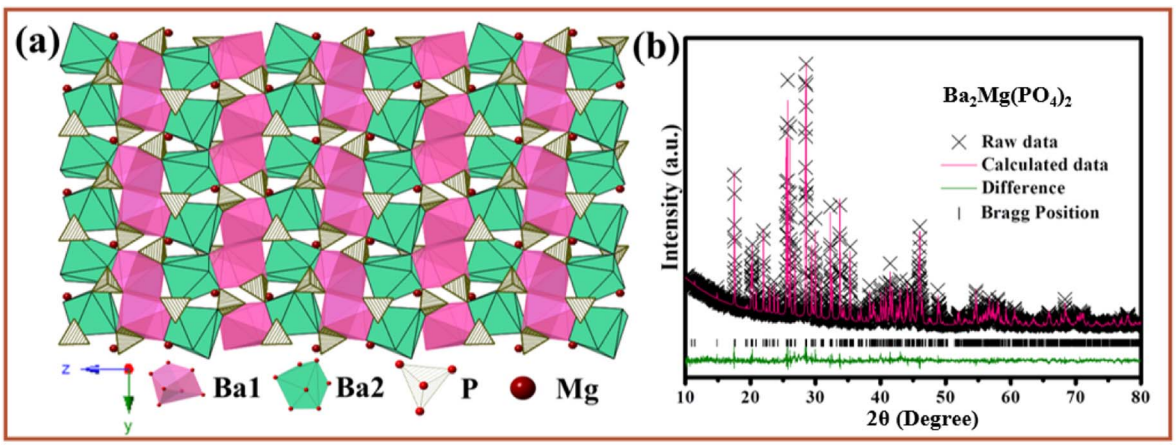

Fig. 1 (a) Crystal structure of $Ba_2Mg(PO_4)_2$. (b) Powder XRD patterns for Rietveld structure analysis of $Ba_2Mg(PO_4)_2$ based on the $Ba_2Mg(PO_4)_2$ ICSD#59253 phase model.

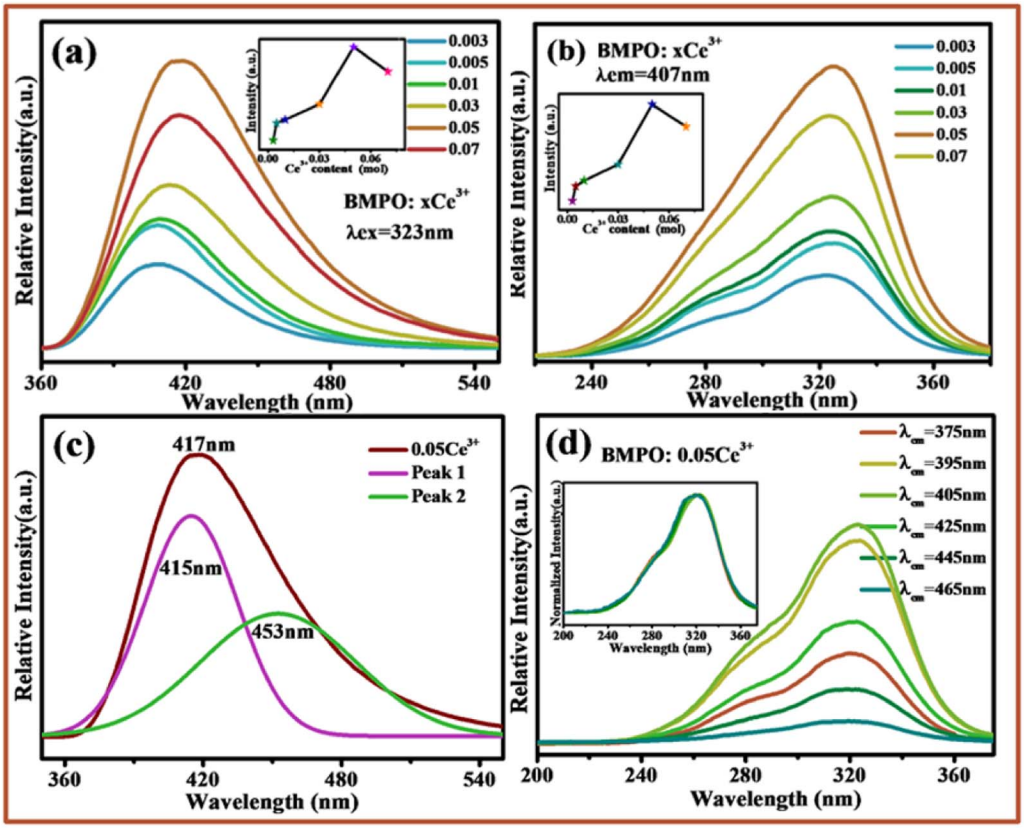

Fig. 2 (a) Excitation spectra of $Ba_2Mg(PO_4)_2$:xCe^{3+} (λ_{em} = 407 nm). (b) Emission spectra of $Ba_2Mg(PO_4)_2$:xCe^{3+} (λ_{ex} = 323 nm). (c) Emission spectra and the two sub-peaks of $Ba_2Mg(PO_4)_2$:$0.05Ce^{3+}$ (λ_{ex} = 323 nm). (d) Excitation spectra of $Ba_2Mg(PO_4)_2$:$0.05Ce^{3+}$ for the different emission wavelengths, the insert describes the normalized excitation spectra.

components with maxima at 415 nm and 453 nm, as shown in Fig. 2c, and the energy difference between the two sub peaks is about 2021 cm^{-1}, which is close to the theoretical energy difference between the $^2F_{7/2}$ and $^2F_{5/2}$ levels. In order to further determine the source of the two sub peaks, the excitation spectra of the sample BMPO:$0.05Ce^{3+}$ at 375 nm, 395 nm, 405 nm, 425 nm, 445 nm and 465 nm were monitored, as shown in Fig. 2d. The inset shows the normalized excitation spectrum. It can be seen from the figure that, except for the difference in luminous intensity, the spectral types of all excitation spectra are completely the same, which indicates that the Ce^{3+} ion is very likely to have only one luminescence center. This proves the asymmetry emission peak of BMPO:$0.05Ce^{3+}$ is caused by the spin–orbit coupling effect of Ce^{3+}.

3.3 Luminescence properties of $Ba_2Mg(PO_4)_2$:Eu^{2+}

Fig. 3a shows the excitation and emission spectra of BMPO:$0.07Eu^{2+}$. Upon excitation at 350 nm, BMPO:$0.07Eu^{2+}$ exhibits a broad emission band extending from 450 nm to 750 nm, and the emission peak is located at about 580 nm due to the $4f^0\,5d^1 \rightarrow 4f^1$ transition of Eu^{2+} ion. Monitored at 580 nm, the excitation spectra give a band with peak center at about 340 nm in the wavelength range of 250–450 nm. Fig. 3b shows the emission spectra of BMPO:yEu^{2+} with different Eu^{2+} concentration. It can be seen that the emission spectra consist of a relatively symmetric broad band center at 580 nm. In order to clarify the influence of Eu^{2+} concentration on its luminescence performance, the normalized emission spectra of BMPO:yEu^{2+} are shown in Fig. 3c, when changed the concentrations of Eu^{2+} ions, the emission spectrum has not changed significantly, and there is no obvious red-blue shift. The emission intensities of BMPO:Eu^{2+} with different Eu^{2+} concentrations are shown in Fig. 3d. The emission intensities firstly increase with increasing the content of Eu^{2+}, the emission intensity is maximized at $x = 0.07$, and then decrease due to the concentration quenching effect.

For BMPO, there are three cation sites, namely Ba_1, Ba_2 and Mg_3. Among them, Ba_1 is surrounded by eight O atoms, Ba_2 is surrounded by seven O atoms, and Mg_3 is surrounded by six oxygen atoms. Taking into account the degree of suitability of the doped ion and the substitute ion in radius and valence, there are only two lattice sites suitable for Eu^{2+} ions to enter, namely Ba_1 and Ba_2 sites. It can be found that the emission spectrum of Eu^{2+} ions is basically symmetrical, which indicates that Eu^{2+} ions are likely to occupy only one of the lattice sites and have only one luminescence center, which results in a relatively symmetrical emission spectrum. In order to clarify the number of luminescence centers, BMPO:$0.07Eu^{2+}$ was subjected to a low-temperature spectrum test at 4 K and a fluorescence lifetime test at room temperature. Fig. 3e shows that the emission spectrum of BMPO:$0.07Eu^{2+}$ has only one relatively

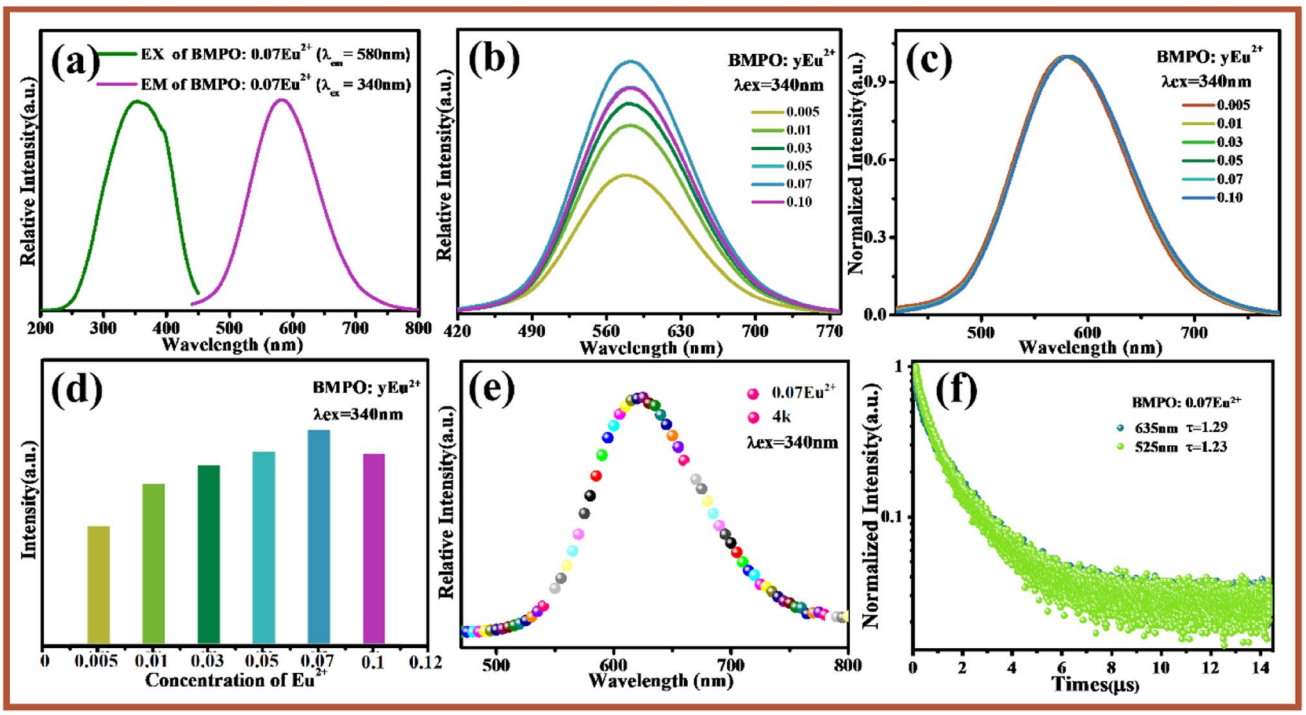

Fig. 3 (a) Excitation spectra and emission spectra of $Ba_2Mg(PO_4)_2$:0.07Eu^{2+}. (b) Emission spectra of $Ba_2Mg(PO_4)_2$:yEu^{2+} (λ_{ex} = 340 nm). (c) The normalized emission spectra of $Ba_2Mg(PO_4)_2$:yEu^{2+}. (d) The emission intensity of $Ba_2Mg(PO_4)_2$:yEu^{2+} with the different concentrations of Eu^{2+} ions. (e) The emission spectrum of $Ba_2Mg(PO_4)_2$:0.07Eu^{2+} at 4 K. (f) The lifetime decay curve at 525 nm and 635 nm emission peaks of $Ba_2Mg(PO_4)_2$:0.07Eu^{2+}.

symmetrical emission peak under the excitation of 340 nm, which proves that there is only one luminescence center. In order to further verify the number of luminescence centers, the decay curves of BMPO:0.07Eu^{2+} monitored at 525 and 635 nm were tested and are presented in Fig. 3f, and the lifetimes of them are 1.23 and 1.29 μs. From the results, it can be seen that the lifetimes of the two emission peaks are almost the same, which further verifies that there is only one luminescence center of Eu^{2+} ions in the BMPO.

Due to the special electronic configuration, Eu^{2+} ion is particularly sensitive to the crystal field environment surrounding the central ion. In order to obtain the detailed structural information of BMPO:yEu^{2+} and find out which lattice site Eu^{2+} ions enter, the structure of BMPO:yEu^{2+} (y = 0–0.1) by GSAS software based on the standard card of BMPO (ICSD#59253) were refined, and shown in Fig. S2 and Table S2.† It can be seen that all parameters meet the experimental requirements, which prove that the refinement results are true and reliable. The evolution of lattice parameters a, b, c and the unit cell volume V of BMPO:yEu^{2+}(y = 0–0.1) is shown in Fig. S3.† It is found that parameters a, b, c and the unit cell volume decrease gradually with the increase of Eu^{2+} content, which is caused by lattice shrinkage caused by Eu^{2+} with smaller radius entering the lattice instead of Ba^{2+} with larger radius. At the same time, it also shows that Eu^{2+} ions are successfully doped in.

As shown in Fig. 4a, the refined crystal structure of BMPO:yEu^{2+}(y = 0–0.1) was analyzed in detail and the volume changes of the lattice sites Ba_1 and Ba_2 were summarized. According to the previous analysis, the radius of Eu^{2+} is smaller than that of Ba^{2+}. If Eu^{2+} successfully occupies a certain lattice site after entering the host, it will definitely cause a change in the volume of this site is shown in Fig. 4b. It can be seen from the Fig. 4a that the volume of Ba_1 gradually decreases with the increase of Eu^{2+} concentration, which is caused by the entry of Eu^{2+} ions with a smaller radius into the site Ba_1, while the volume of Ba_2 shows a slight increase first and then a slight decrease. Through analysis, it is found that the lattice sites Ba_1 and Ba_2 are connected to each other through the sides and apex angles. When Eu^{2+} ions enter the Ba_1 lattice site, the unit cell volume of Ba_1 decreases, and the decrease of Ba_1 also has a pulling effect on Ba_2, so that the volume of Ba_2 increases slightly. When the doping concentration of Eu^{2+} ions is large, it cannot completely enter the Ba_1 site, and part of it will enter the gap in the lattice site, and the Eu^{2+} ions that enter the gap will Ba_1 has a certain degree of squeezing effect, hence its unit cell volume is slightly reduced. In summary, Eu^{2+} ions do occupy the Ba_1 site after entering the BMPO.

3.4 Luminescence properties of BMPO:0.05Ce^{3+}, yEu^{2+}

Fig. 5a shows the emission spectra of BMPO:0.05Ce^{3+}, yEu^{2+} under excitation at 323 nm. Due to the 5d → 4f transition of Ce^{3+} and Eu^{2+}, there are two emission bands from 370 nm to 520 nm with a peak at 407 nm, and from 540 nm to 720 nm with a peak at 580 nm. With increasing the concentration of Eu^{2+}, the emission intensity of Ce^{3+} decreases monotonically. Meanwhile, the emission intensity of Eu^{2+} increases gradually until the Eu^{2+}

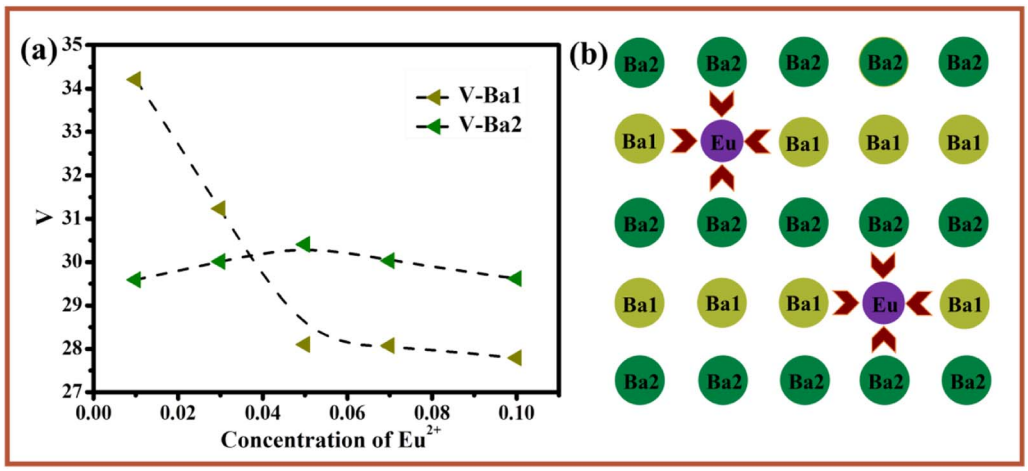

Fig. 4 (a) The lattice volume Ba_1 and Ba_2 with Eu^{2+} doping concentration in $Ba_2Mg(PO_4)_2$:yEu^{2+}. (b) Schematic diagram of the lattice change after Eu^{2+} enters the host.

content is $x = 0.07$ and the concentration quenching occurs is shown in Fig. 5b. In addition, the emission spectra of Ce^{3+} and excitation spectra of Eu^{2+} are also shown in Fig. 5c. A significant spectral overlap between the emission spectrum of BMPO:0.05Ce^{3+} and the excitation spectrum of BMPO:0.07Eu^{2+} is observed, which indicates that the energy transfer from the Ce^{3+} to Eu^{2+} ions can be expected in BMPO.

To further validate the energy transfer process between Ce^{3+} and Eu^{2+}, the decay curves of Ce^{3+} fluorescence lifetime for BMPO:0.05Ce^{3+}, yEu^{2+} were measured by monitoring at 407 nm with the excitation at 323 nm, and the measured decay curves are depicted in Fig. 6a. It is found that all the decay curves can be well fitted with a second-order exponential decay, which can be fitted using the eqn (1):[38–40]

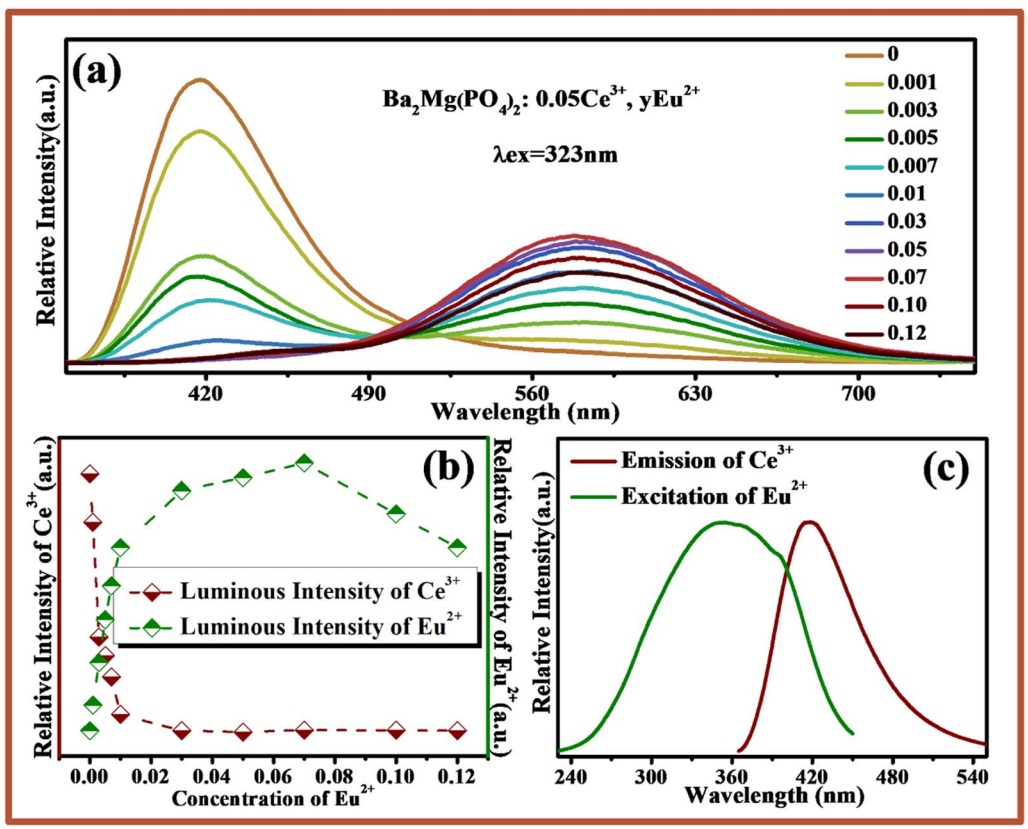

Fig. 5 (a) The emission spectra of $Ba_2Mg(PO_4)_2$:0.05Ce^{3+}, yEu^{2+} (λ_{ex} = 323 nm). (b) The luminous intensity of Eu^{2+} and Ce^{3+} varies with the concentration of Eu^{2+} ions. (c) The emission spectra of $Ba_2Mg(PO_4)_2$:0.05Ce^{3+} and the excitation spectra of $Ba_2Mg(PO_4)_2$:0.07Eu^{2+}.

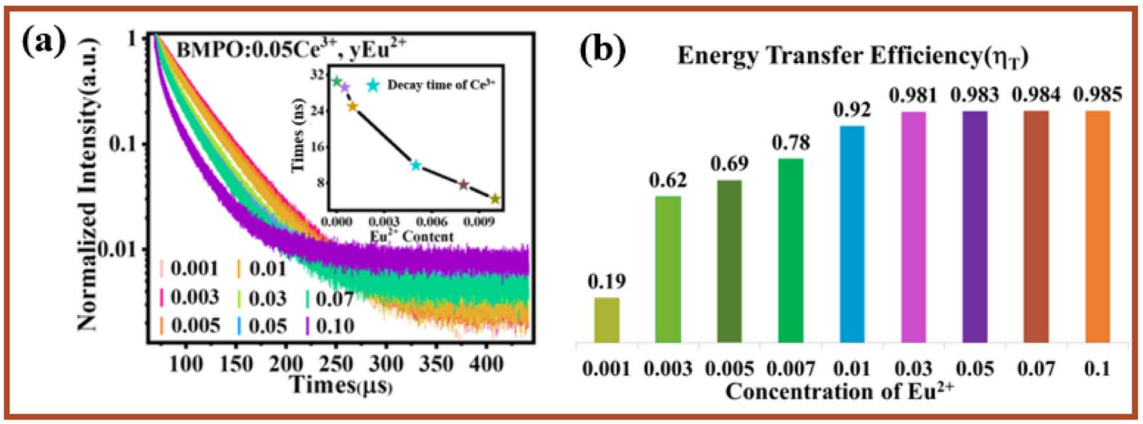

Fig. 6 (a) Decay curves of Ce^{3+} ions in $Ba_2Mg(PO_4)_2$:0.05Ce^{3+}, yEu^{2+} (λ_{ex} = 320 nm). (b) The energy transfer efficiency between Ce^{3+}–Eu^{2+} in $Ba_2Mg(PO_4)_2$:0.05Ce^{3+}, yEu^{2+}.

$$I(t) = I_0 + A_1\exp(-t/\tau_1) + A_2\exp(-t/\tau_2) \quad (1)$$

where I is luminescence intensity, A_1 and A_2 are constants, τ is average lifetime, and τ_1 and τ_2 are lifetime for rapid and slow decays, respectively. The average lifetime τ^* can be obtained using the formula (2):[38–40]

$$\tau^* = (A_1\tau_1^2 + A_2\tau_2^2)/(A_1\tau_1 + A_2\tau_2) \quad (2)$$

The effective decay time (τ^*) of Ce^{3+} ions were calculated to be 32.0170, 30.5329, 29.2241, 25.0169, 11.9310, 8.3924, 7.5280 and 4.4988 ns, respectively. Obviously, the lifetime values decreased monotonically as the Eu^{2+} concentration increased, which strongly demonstrates energy transfer from Ce^{3+} to Eu^{2+}. In addition, the energy transfer efficiency (η_T) can be calculated using the following eqn (3).[41–43]

$$\eta_T = 1 - (I_s - I_{s0}) \quad (3)$$

where I_s and I_{s0} are luminescence intensity of sensitizer Ce^{3+} in the presence and absence of activator Eu^{2+}. As shown in Fig. 6b, the energy-transfer efficiency increased sharply with the increasing of the Eu^{2+} content. The η_T value reached 98.5% at y = 0.1, which also indicated that the energy transfer efficiency of Ce^{3+}–Eu^{2+} can increase with increasing Eu^{2+} content.

Based on the above argument, there are the energy transfer from Ce^{3+} to Eu^{2+} ions, hence the determination of their energy transfer mechanism is also an important factor to study their energy transfer process. In general, the exchange interaction and multipolar interaction are the main types of interactions between sensitizer and activator.[44] With the increase of activator concentration, the distance between the sensitizer and the activator begins to approach, and there is an obvious energy transfer between the sensitizer and the activator. When the distance reaches the critical value, the energy transfer will be hindered. The critical distance R_{Ce-Eu} between Ce^{3+} and Eu^{2+} can be estimated by[45,46]

$$R_c = 2\left[\frac{3V}{4\pi X_c N}\right]^{\frac{1}{3}} \quad (4)$$

where V is the volume in the unit cell, N is the number of cations in the unit cell, X_c is the total concentration of Ce^{3+} ions and the

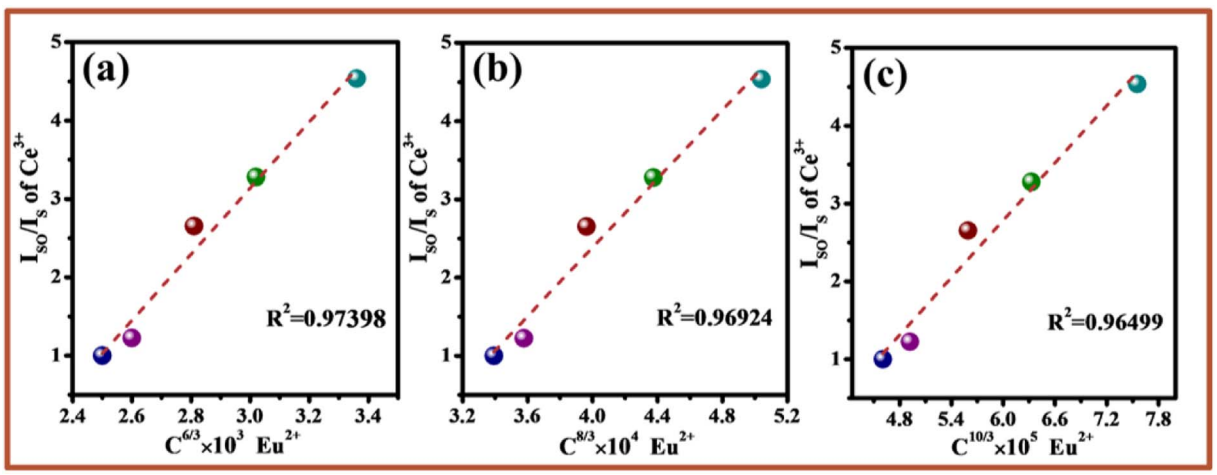

Fig. 7 Relationships between I_{s0}/I_s and $C^{n/3}$: (a) n = 6, (b) n = 8, (c) n = 10.

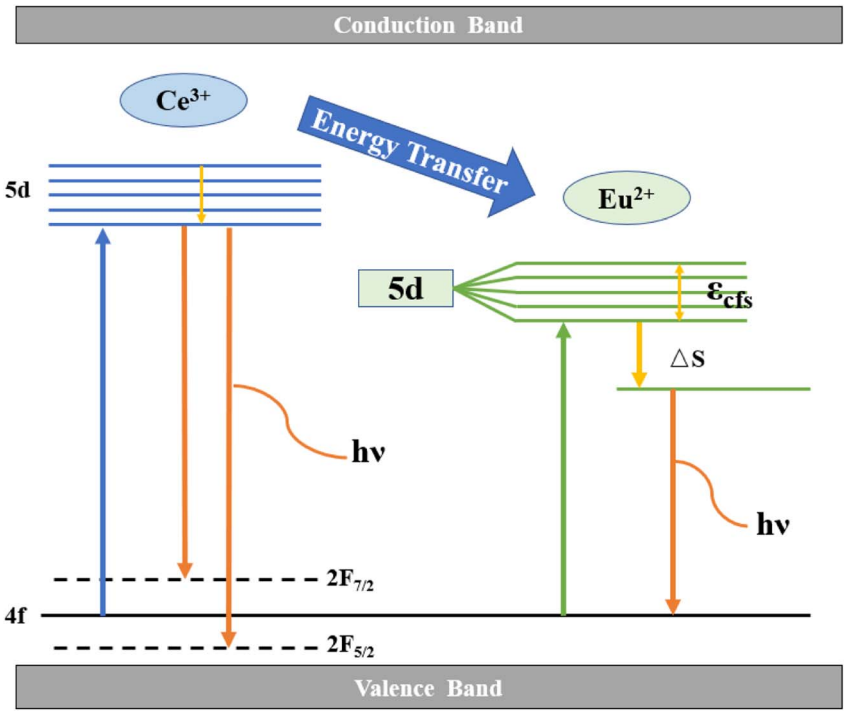

Fig. 8 Energy level scheme for ET in $Ba_2Mg(PO_4)_2$:0.05Ce^{3+}, yEu^{2+}.

critical concentration of Eu^{2+}. For BMPO host, the value of V is 758.43 Å^3 and $N = Z = 4$, the critical concentration of Eu^{2+} is 0.07. The critical distance of energy transfer is calculated to be about 14.3 Å for BMPO:0.05Ce^{3+}, yEu^{2+}, which is larger than the critical distance for exchange interaction (5 Å). Therefore, the interaction between Ce^{3+} and Eu^{2+} ions in BMPO might take place *via* multipolar interaction.

On the basis of Dexter's the formula of multipolar interaction and Reisfeld's approximation, the following relationship (5) can be obtained:[47]

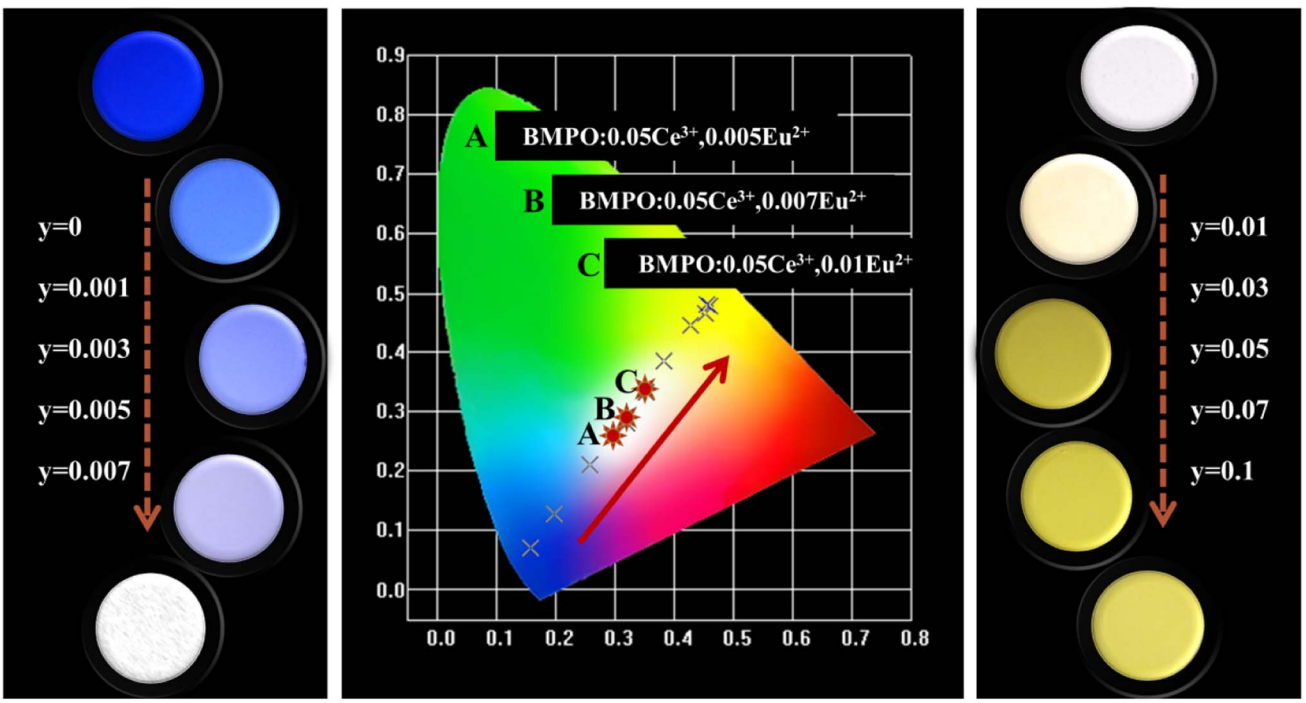

Fig. 9 The color coordinates and photographs of $Ba_2Mg(PO_4)_2$:0.05Ce^{3+}, yEu^{2+} (λ_{ex} = 365 nm).

$$\frac{I_{SO}}{I_S} \propto C_{ln^{2+}}^{n/3} \quad (5)$$

where I_{SO} and I_S are the luminescence intensity of Ce^{3+} in the absence and presence of Eu^{2+}, C is the total doping content of sensitizer (Ce^{3+}) and activator (Eu^{2+}), and $n = 6$, 8, 10 corresponds to the dipole–dipole, dipole–quadrupole, and quadrupole–quadrupole interactions, respectively. The relationship of $\frac{I_{SO}}{I_S} \propto C_{ln^{2+}}^{n/3}$ is shown in Fig. 7a–c. Considering the fitting factor R^2, the relation $\frac{I_{SO}}{I_S} \propto C_{ln^{2+}}^{6/3}$ has the best fitting, implying that the energy transfer between Ce^{3+} and Eu^{2+} in BMPO occurs *via* a dipole–dipole interaction mechanism.

Fig. 8 describes the energy level transitions of Ce^{3+} and Eu^{2+} ions and the energy transfer mechanism of Ce^{3+}–Eu^{2+} in BMPO. Under the 323 nm excitation, the electrons of Ce^{3+} ions transition from the 4f energy level to the 5d energy level. Because the exposed 5d orbital of Ce^{3+} is susceptible to splitting by the crystal field, and it has two ground states the electron configurations are $2F_{7/2}$ and $2F_{5/2}$, respectively, hence they show a relatively wide emission range. At the same time, because the upper energy level of Eu^{2+} ions is lower than that of Ce^{3+} ions, they are excited to the 5d energy level. A part of the electrons will jump to the upper energy level of Eu^{2+} ion, and then return to the lower energy level and emit photon. Where ε_{cfs} denotes the 5d energy level cleavage of Eu^{2+} and ΔS is the Stokes shift, which is the energy transfer process of Ce^{3+}–Eu^{2+}.

The chromaticity calculation was performed based on the luminescence spectra of BMPO:0.05Ce^{3+}, $y$$Eu^{2+}$ under the 323 nm excitation, and the calculation results of the CIE coordinates and a series of digital photographs upon the 365 nm UV lamp are shown in Fig. 9. As the doping concentrations of Eu^{2+} ions are from 0 to 0.1, the color coordinates (x, y) of BMPO:0.05Ce^{3+}, $y$$Eu^{2+}$ shift from blue (0.157, 0.071) to yellow (0.452, 0.466). It is worth noting that the CIE chromaticity coordinates of BMPO:0.05Ce^{3+}, 0.005Eu^{2+}, BMPO:0.05Ce^{3+}, 0.007Eu^{2+} and BMPO:0.05Ce^{3+}, 0.01Eu^{2+} are (0.294, 0.257), (0.319, 0.279) and (0.352, 0.332), which are all located in the white light region. The results indicate that BMPO:0.05Ce^{3+}, $y$$Eu^{2+}$ can be achieved by appropriately adjusting the ratio of Ce/Eu ions.

4. Conclusions

In summary, series color-tunable and single-composition white emitting phosphors BMPO:0.05Ce^{3+}, $y$$Eu^{2+}$ were successfully synthesized. The samples could get varied color emission from blue (0.157, 0.071) towards white (0.352, 0.332) and ultimately to yellow (0.452, 0.466) under the excitation of 323 nm light by precisely controlling the relative proportion of Ce^{3+}/Eu^{2+}. The energy transfer from Ce^{3+} to Eu^{2+} in BMPO has been validated and the energy transfer mechanism is the dipole–dipole interaction. The results proved that the single-phased white emitting phosphor BMPO:$x$$Ce^{3+}$, $y$$Eu^{2+}$ can be excited by UV-LED chips and has the potential application in white LEDs.

Conflicts of interest

The authors declare no competing financial interest.

Acknowledgements

The work is supported by the National Natural Science Foundation of China (No. 61805285).

References

1 G. Li, Y. Tian, Y. Zhao and J. Lin, Recent Progress in Luminescence tuning of Ce^{3+} and Eu^{2+}-activated phosphors for PC W-LEDs, *Chem. Soc. Rev.*, 2015, **44**, 8688–8713.
2 J. Zhao, X. Sun and Z. Wang, Ce^{3+}/Eu^{2+} doped $SrSc_2O_4$ phosphors: synthesis, luminescence and energy transfer from Ce^{3+} to Eu^{2+}, *Chem. Phys. Lett.*, 2018, **691**, 68–72.
3 W. Lv, J. Huo, Y. Feng, S. Zhao and H. You, Photoluminescence, energy transfer and tunable color of Ce^{3+}, Tb^{3+} and Eu^{2+} activated oxynitrides phosphor with high brightness, *Dalton Trans.*, 2016, **45**(23), 9676–9683.
4 J. Ha, Z. Wang, E. Novitskaya, G. A. Hirata, O. A. Graeve, S. P. Ong and J. McKittrick, An integrated first principles and experimental investigation of the relationship between structural rigidity and quantum efficiency in phosphors for solid state lighting, *J. Lumin.*, 2016, **179**, 297–305.
5 C. Guo, Y. Xu, F. Lv and X. Ding, Luminescent properties of Sr_2SiO_4:Eu^{2+} nanorods for near-UV white LED, *J. Alloys Compd.*, 2010, **497**(1–2), L21–L24.
6 G. Li, Y. Fan, H. Guo and Y. Wang, Synthesis, structure and photoluminescence properties of Ce^{3+}-doped $SrSc_2O_4$: a new scandate green-emitting phosphor with blue excitation, *New J. Chem.*, 2017, **41**, 5565–5571.
7 C. Guo, M. Li, Y. Xu, T. Li, Z. Ren and J. Bai, A potential green-emitting phosphor $Ca_8Mg(SiO_4)_4Cl_2$:Eu^{2+} for white light emitting diodes prepared by sol-gel method, *Appl. Surf. Sci.*, 2011, **257**(21), 8836–8839.
8 G. Li, Y. Zhao, Y. Wei, Y. Tian, Z. Quan and J. Lin, Novel yellowish-green light-emitting $Ca_{10}(PO_4)_6O$: Ce^{3+} phosphor: structural refinement, preferential site occupancy and color tuning, *Chem. Commun.*, 2016, **52**, 3376–3379.
9 J. Xiang, J. Zheng, Z. Zhou, H. Suo, X. Zhao, X. Zhou, N. Zhang, M. S. Molokeev and C. Guo, Enhancement of red emission and site analysis in Eu^{2+} doped new-type structure $Ba_3CaK(PO_4)_3$ for plant growth white LEDs, *Chem. Eng. J.*, 2019, **356**, 236–244.
10 K. Uheda, N. Hirosaki, Y. Yamamoto, A. Naito, T. Nakajima and H. Yamamoto, Luminescence properties of a red phosphor, $CaAlSiN_3$:Eu^{2+}, for white light-emitting diodes, *Electrochem. Solid-State Lett.*, 2006, **9**, H22–H25.
11 P. Li, Z. Wang, Z. Yang and Q. Guo, $Ba_2B_2O_5$:Ce^{3+}: a novel blue emitting phosphor for white LEDs, *Mater. Res. Bull.*, 2014, **60**, 679–681.
12 Q. Wu, Z. Yang, Z. Zhao, M. Que, X. Wang and Y. Wang, Synthesis, crystal structure and luminescence properties of a $Y_4Si_2O_7N_2$: Ce^{3+} phosphor for near-UV white LEDs, *J. Mater. Chem. C*, 2014, **2**, 4967–4973.

13 R. Yu, C. Guo, T. Li and Y. Xu, Preparation and luminescence of blue-emitting phosphor Ca_2PO_4Cl: Eu^{2+} for n-UV white LEDs, *Curr. Appl. Phys.*, 2013, **13**(5), 880–884.

14 W. Geng, X. Zhou, J. Ding, G. Li and Y. Wang, $K_7Ca_9[Si_2O_7]_4F:Ce^{3+}$: a novel blue-emitting phosphor with good thermal stability for ultraviolet-excited light emitting diodes, *J. Mater. Chem. C*, 2017, **5**, 11605–11613.

15 X. Ding and Y. Wang, Structure and photoluminescence properties of a novel apatite green phosphor $Ba_5(PO_4)_2SiO_4$: Eu^{2+} excited by NUV light, *Phys. Chem. Chem. Phys.*, 2017, **19**, 2449–2458.

16 X. Wang, Z. Zhao, Q. Wu, C. Wang, Q. Wang, Y. Li and Y. Wang, Structure, photoluminescence and abnormal thermal quenching behavior of Eu^{2+}-doped $Na_3Sc_2(PO_4)_3$: a novel blue-emitting phosphor for n-UV LEDs, *J. Mater. Chem. C*, 2016, **4**, 8795–8801.

17 X. Wang, Z. Zhao, Q. Wu, Y. Li and Y. Wang, Synthesis, structure and photoluminescence properties of $Ca_2LuHf_2(AlO_4)_3$: Ce^{3+}, a novel garnet-based cyan lightemitting phosphor, *J. Mater. Chem. C*, 2016, **4**, 11396–11403.

18 Y. Liu, J. Zhang, C. Zhang, J. Xu, G. Liu, J. Jiang and H. Jiang, $Ba_9Lu_2Si_6O_{24}$: Ce^{3+}: An Efficient Green Phosphor with High Thermal and Radiation Stability for Solid-State Lighting, *Adv. Opt. Mater.*, 2015, **3**(8), 1096–1101.

19 Z. Wang, B. Yang, P. Li, Z. Yang and Q. Guo, Energy transfer between activators at different crystallographic sites in Sr_3SiO_5: Eu^{2+}, *Physica B*, 2012, **407**(8), 1282–1286.

20 M. Zhang, J. Wang, Q. Zhang, W. Ding and Q. Su, Optical properties of $Ba_2SiO_4:Eu^{2+}$ phosphor for green light emitting diode (LED), *Mater. Res. Bull.*, 2007, **42**, 33–39.

21 W. Lv, Y. Jia, Q. Zhao, M. Jiao, B. Shao, W. Lu and H. You, Crystal Structure and Luminescence Properties of $Ca_8Mg_3Al_2Si_7O_{28}$: Eu^{2+} for WLEDs, *Adv. Opt. Mater.*, 2014, **2**, 183–188.

22 M. Zhao, Z. Xia, M. S. Molokeev, L. Ning and Q. Liu, Temperature and Eu^{2+} doping induced phase selection in $NaAlSiO_4$ polymorphs and the controlled yellow/blue emission, *Chem. Mater.*, 2017, **29**, 6552–6559.

23 Z. Xia, R. Liu, K. Huang and V. Drozd, $Ca_2Al_3O_6F$: Eu^{2+}: a green-emitting oxyfluoride phosphor for white lightemitting diodes, *J. Mater. Chem.*, 2012, **22**, 15183–15189.

24 J. Qiao, L. Ning, M. S. Molokeev, Y. Chuang, Q. Liu and Z. Xia, Eu^{2+} site preferences in the mixed cation $K_2BaCa(PO_4)_2$ and thermally stable luminescence, *J. Am. Chem. Soc.*, 2018, **140**(30), 9730–9736.

25 W. Sun, Y. Jia, R. Pang, H. Li, T. Ma, D. Li, J. Fu, S. Zhang, L. Jiang and C. Li, $Sr_9Mg_{1.5}(PO_4)_7$: Eu^{2+}: a novel broadband orange-yellow-emitting phosphor for blue light-excited warm white LEDs, *ACS Appl. Mater. Interfaces*, 2015, **7**(45), 25219–25226.

26 D. Zhao, S.-R. Zhang, Y.-P. Fan, B.-Z. Liu and R.-J. Zhang, Thermally stable phosphor $KBa_2(PO_3)_5$: Eu^{2+} with broadband cyan emission caused by multisite occupancy of Eu^{2+}, *Inorg. Chem.*, 2020, **59**, 8789–8799.

27 S. Liang, P. Dang, G. Li, M. S. Molokeev, Y. Wei, Y. Wei, H. Lian, M. Shang, A. A. Al Kheraiff and J. Lin, Controllable two-dimensional luminescence tuning in Eu^{2+}, Mn^{2+} doped $(Ca,Sr)_9Sc(PO_4)_7$ based on crystal field regulation and energy transfer, *J. Mater. Chem. C*, 2018, **6**, 6714–6725.

28 C. Wang, P. Li, Z. Wang, Y. Sun, J. Cheng, Z. Li, M. Tian and Z. Yang, Crystal structure, luminescence properties, energy transfer and thermal properties of a novel color-tunable, white light-emitting phosphor $Ca_{9-x-y}Ce(PO_4)_7$:$x$$Eu^{2+}$, y$Mn^{2+}$, *Phys. Chem. Chem. Phys.*, 2016, **18**, 28661–28673.

29 X. Li, P. Li, C. Liu, L. Zhang, Z. Xing, Z. Yang and Z. Wang, Tuning the luminescence of $Ca_9La(PO_4)_7$: Eu^{2+} *via* artificially inducing potential luminescence centers, *J. Mater. Chem. C*, 2019, **7**, 14601–14611.

30 X. Fu, S. Zheng, Y. Liu and H. Zhang, Yellow phosphors $Ba_2Mg(Po_4)_2$: Eu^{2+} fit for white light-emitting diodes prepared with sol-gel precursor route, *J. Lumin.*, 2018, **206**, 120–124.

31 S. K. Ramteke, N. S. Kokode, A. N. Yerpude, G. N. Nikhare and S. J. Dhoble, Synthesis and photoluminescence properties of Eu^{3+} activated $Ba_2Mg(Po_4)_2$ phosphor, *J. Lumin.*, 2020, **35**(4), 618–621.

32 Q. Hu, Z. Pan, Y. Xu, L. Wang and L. Ning, Dopant site environment and spectrum blue shift of yellow-emitting solid solution phosphor $Ba_{2x}Sr_xMg(Po_4)_2:Eu^{2+}$, *J. Am. Ceram. Soc.*, 2016, **99**(2), 645–650.

33 H. Song, C. Lee, S. Hwang and I. Cho, Wet-chemical preparation of barium magnesium orthophosphate, $Ba_2Mg(Po_4)_2:Eu^{2+}$, nanorod phosphor with enhanced optical and photoluminescence properties, *RSC Adv.*, 2016, **6**, 61378–61385.

34 S. Xu, K. Tang, D. Zhu and T. Han, Luminescence properties and energy transfer of $Ba_2Mg(PO_4)_2:Eu^{2+}$, Mn^{2+} phosphor synthesized by co-precipitation method, *Opt. Mater.*, 2015, **42**, 106–110.

35 Z. Yang, S. Ma, H. Yu, F. Wang, X. Ma, Y. Liu and P. Li, Luminescence studies of $Ba_{1-x}Mg_{2-y}(Po_4)_2$:$x$$Eu^{2+}$, $y$$Mn^{2+}$ phosphor, *J. Alloys Compd.*, 2011, **509**, 76–79.

36 J. Zhang, B. Ji and H. Zheng, Investigations on the luminescence of $Ba_2Mg(PO_4)_2:Eu^{2+}$, Mn^{2+} phosphors for LEDs, *Opt. Mater. Express*, 2016, **6**(11), 3470–3475.

37 Q. S. Hu, Z. F. Pan, Y. Xu., L. L. Wang and L. X. Ning, Dopant Site Environment and Spectrum Blue Shift of Yellow-Emitting Solid Solution Phosphor $Ba_{2-x}Sr_xMg(PO_4)_2:Eu^{2+}$, *J. Am. Ceram. Soc.*, 2016, **99**(2), 645–650.

38 X. Zhang, J. Xu, Z. Guo and M. Gong, Luminescence and energy transfer of dual-emitting solid solution phosphors $(Ca, Sr)_{10}Li(PO_4)_7$: Ce^{3+}, Mn^{2+} for ratiometric temperature sensing, *Ind. Eng. Chem. Res.*, 2017, **56**, 890–898.

39 M. Li, J. Zhang, J. Han, Z. Qiu, W. Zhou, L. Yu, S. Lian and Z. Li, Changing Ce^{3+} content and codoping Mn^{2+} induced tunable emission and energy transfer in $Ca_{2.5}Sr_{0.5}Al_2O_6$: Ce^{3+}, Mn^{2+}, . *Inorg. Chem.*, 2017, **56**, 241–251.

40 K. Li, H. Lian, M. Shang and J. Lin, A novel greenish yellow-orange red $Ba_3Y_4O_9$: Bi^{3+}, Eu^{3+} phosphor with efficient energy transfer for UV-LEDs, *Dalton Trans.*, 2015, **44**, 2054–20550.

41 W. Yang and T. Chen, White-light generation and energy transfer in $SrZn_2(PO_4)_2$: Eu, Mn phosphor for ultraviolet light-emitting diodes, *Appl. Phys. Lett.*, 2006, **88**, 101903.

42 K. H. Kwon, W. B. Im, H. S. Jang, H. S. Yoo and D. Y. Jeon, Luminescence properties and energy transfer of site-sensitive $Ca_{6-x-y}Mg_{x-z}(PO_4)_4$: yEu^{2+}, zMn^{2+} phosphors and their application to near-UV LED based white LEDSs, *Inorg. Chem.*, 2009, **48**, 11525–11532.

43 G. Li, Y. Zhang, D. Geng, M. Shang, C. Peng, Z. Cheng and J. Lin, Single-composition trichromatic white-emitting $Ca_4Y_6(SiO_4)_6O$:Ce^{3+}/Mn^{2+}/Tb^{3+} phosphor: luminescence and energy transfer, *ACS Appl. Mater. Interfaces*, 2012, **4**, 296–305.

44 D. L. Dexter and J. H. Schulman, Theory of concentration quenching in inorganic phosphors, *J. Chem. Phys.*, 1954, **22**(6), 1063–1070.

45 D. Geng, G. Li, M. Shang, D. Yang, Y. Zhang, Z. Cheng and J. Lin, Color tuning *via* energy transfer in $Sr_3In(PO_4)_3$:Ce^{3+}/Tb^{3+}/Mn^{2+} phosphors, *J. Mater. Chem.*, 2012, **22**(28), 14262–14271.

46 M. Cui, J. Wang, J. Li, S. Huang and M. Shang, An abnormal yellow emission and temperature-sensitive properties for perovskite-type Ca_2MgWO_6 phosphor *via* cation substitution and energy transfer, *J. Lumin.*, 2019, **214**, 116588.

47 M. Shang, G. Li, D. Geng and D. Yang, J. Lin. Blue emitting $Ca_8La_2(PO_4)_6O_2$:Ce^{3+}/Eu^{2+} phosphors with high color purity and brightness for White LED: Soft-chemical synthesis, luminescence, and energy transfer properties, *J. Phys. Chem. C*, 2012, **116**(18), 10222–10231.